Endocytosis-dependent coordination of multiple actin regulators is required for wound healing

Yutaka Matsubayashi, Camilla Coulson-Gilmer, and Tom H. Millard

The Healing Foundation Centre, Faculty of Life Sciences, University of Manchester, Manchester M13 9PT, England, UK

The ability to heal wounds efficiently is essential for life. After wounding of an epithelium, the cells bordering the wound form dynamic actin protrusions and/or a contractile actomyosin cable, and these actin structures drive wound closure. Despite their importance in wound healing, the molecular mechanisms that regulate the assembly of these actin structures at wound edges are not well understood. In this paper, using *Drosophila melanogaster* embryos, we demonstrate that Diaphanous, SCAR, and WASp play distinct but overlapping roles in regulating actin assembly during wound healing. Moreover, we show that endocytosis is essential for wound edge actin assembly and wound closure. We identify adherens junctions (AJs) as a key target of endocytosis during wound healing and propose that endocytic remodeling of AJs is required to form "signaling centers" along the wound edge that control actin assembly. We conclude that coordination of actin assembly, AJ remodeling, and membrane traffic is required for the construction of a motile leading edge during wound healing.

Introduction

Epithelia provide essential protection against infective agents, toxins, and fluid loss; therefore, it is vital that damaged epithelia are rapidly repaired. After injury, epithelial cells surrounding the wound move into the gap until the opposing epithelial edges meet and fuse, thus reestablishing epithelial integrity. The actin cytoskeleton of the cells surrounding the wound provides the main driving force for epithelial wound closure and can drive closure by two distinct mechanisms. First, wound edge cells can form actin protrusions, i.e, lamellipodia and filopodia, which are used to crawl over the substratum, probe the environment and/or interact and adhere with cells from opposing wound edge. Second, a contractile cable composed of actin and myosin II can assemble around the wound edge, linked from one cell to the next by adherens junctions (AJs). Contraction of this cable pulls the wound closed in the manner of a purse string. Purse string wound closure is the primary mechanism of epithelial repair in embryonic tissues but is also believed to contribute to repair of adult tissues including the cornea and gut (Martin and Parkhurst, 2004; Matsubayashi and Millard, 2013). Despite its widespread importance in the maintenance of epithelial tissues, the molecular mechanisms that underlie actin remodeling during wound closure remain largely unknown.

The *Drosophila melanogaster* embryo has emerged as an excellent model system for studying wound closure in vivo as it is genetically tractable and amenable to live imaging of the various cell activities associated with healing, including the formation of the actin protrusions and contractile cable that drive closure. Using this system, some of the upstream signals that trigger wound edge actin assembly have been identified. For example, the kinases Stitcher and Src are required for wound edge actin assembly, and the GTPases Rho and Cdc42 regulate formation of the actin cable and protrusions, respectively (Wood et al., 2002; Wang et al., 2009; Tsarouhas et al., 2014). However, the identity of the actin regulators that drive actin assembly at wound edges downstream of these signaling proteins remains largely unknown. Assembly of actin filaments is usually initiated by actin nucleators, of which there are two main classes: the Arp2/3 complex and formins. The Arp2/3 complex mediates the formation of the network of branched F-actin, whereas formins including Diaphanous (Dia) induce the formation of unbranched actin filaments. The Arp2/3 complex requires activator proteins such as SCAR/WAVE and WASp (Wiskott-Aldrich Syndrome protein) to nucleate actin filaments (Millard et al., 2004; Mattila and Lappalainen, 2008; Krause and Gautreau, 2014). With the exception of Dia, which is reported to play a role in the repair of the *Drosophila* pupal epidermis (Antunes et al., 2013), the roles of these proteins in wound healing in vivo have not been studied.

AJs are a key component of wound edge actin cables, as they link the cable from one cell to the next. The AJs along the wound edge undergo changes in composition and appearance after wounding, and this remodeling has been proposed to be important in triggering wound responses (Pickering et al., 2013; Carvalho et al., 2014; Tsarouhas et al., 2014; Zulueta-Coarasa

Correspondence to Tom H. Millard: tom.millard@manchester.ac.uk

Abbreviations used in this paper: AJ, adherens junction; Dia, Diaphanous; DN, dominant negative; p120ctn, p120-catenin; *shg*, *shotgun*; *shi*, *shibire*; TCJ, tricellular junction.

The Rockefeller University Press $30.00
J. Cell Biol. Vol. 210 No. 3 419–433
www.jcb.org/cgi/doi/10.1083/jcb.201411037

et al., 2014). Remodeling of AJs occurs by endocytic recycling (Georgiou et al., 2008; Leibfried et al., 2008; Levayer et al., 2011), raising the possibility that membrane trafficking processes may also be important for wound responses; however, this has not been investigated.

In this study, we explore the dynamics and regulation of actin assembly during wound healing in *Drosophila* embryos and find that different actin regulators play distinct roles in assembling actin at wound edges. We identify links between actin assembly and endocytosis at the wound edge and show that endocytosis is essential for wound healing. AJs are identified as the likely target of endocytosis at wound edges. We suggest that endocytic remodeling of AJs creates a signaling platform that coordinates actin dynamics at wound edges.

Results

Actin assembly at wound edges initiates at sites that were formerly tricellular junctions (TCJs)

F-actin structures formed at wound edges are believed to be the main driver of epithelial wound healing; however, the mechanisms by which these structures are assembled during wound healing in vivo are poorly understood. To address this question, we used the ventral epidermis of stage 15 *Drosophila* embryos wounded with an ablation laser as a model system. By expressing the F-actin marker GFP-Moesin in the embryonic epidermis, we were able to live image actin dynamics throughout the closure process (Fig. 1 A). As previously observed (Wood et al., 2002), wound edge cells assemble an actin cable around the wound edge and actin protrusions that project into the wound. We noticed, however, that the formation of these actin structures was preceded by the assembly of punctate actin structures <2 µm in size along the wound edge (Fig. 1 A). Closer scrutiny of these early, punctate assemblies (henceforth, actin puncta) in embryos expressing the F-actin probe mCherry-Moesin alongside E-cadherin–GFP revealed that they predominantly formed at sites which had been TCJs before wounding (83%, or 52 out of 63 puncta from five wounds; Fig. 1 B). TCJs are specialized structures found at the intersection of three cells (Schulte et al., 2003; Ikenouchi et al., 2005; Lye et al., 2014). After wounding, these structures cannot be considered TCJs any longer, as one or two of the three cells has been removed, so we will henceforth describe these wound edge structures as former-TCJs. Where two of the three cells that surrounded the TCJ remain intact after wounding, these junction sites ultimately develop into enlarged bulb-like AJs that link the wound edge actin cable from cell to cell (Fig. 1, B and C; Danjo and Gipson, 1998; Wood et al., 2002). We also examined the dynamics of myosin at the wound edge in the early stages of wound closure, by expressing GFP-Zipper (myosin II heavy chain) in the epidermis. Like actin, myosin accumulated at former-TCJs along the wound edge, colocalizing with the actin puncta (Fig. 1 D, arrowheads). These myosin puncta then enlarge and extend "arms" toward their neighbors (Fig. 1 D, arrows), eventually forming a continuous cable encircling the wound (Fig. 1 D, 5:30; and Video 1). Former-TCJs therefore appear to be the major sites at which both actin assembly and myosin recruitment are initiated during wound healing.

We then analyzed the prevalence of actin puncta, actin protrusions, and actin cable throughout wound closure in embryos expressing GFP-Moesin in the epidermis. To do this, we measured the number of puncta per unit length and the proportion of the wound circumference occupied by cable or protrusions throughout closure (see Materials and methods for quantitation procedures). Actin puncta increased until around 10 min after wounding and then gradually declined (Fig. 1 E). Actin cable and protrusions assembled with similar dynamics to one another, gradually increasing over the first 20 min after wounding and then remaining broadly constant until closure was complete (Fig. 1 E). We next correlated actin assembly with wound closure progress. Consistent with previous studies, we found that wound closure commences at around 5 min after wounding, proceeds rapidly for the next 30 min and is complete after ∼60 min (Fig. 1 F; Wood et al., 2002; Abreu-Blanco et al., 2012; Fernandez-Gonzalez and Zallen, 2013). The dynamics of closure were broadly consistent for wounds ranging from 200–1,000 µm^2 in area (Fig. 1 F). Comparison of the time courses of actin remodeling and wound closure indicates that the levels of actin cable and protrusions correlate reasonably well with the progression of closure, whereas formation of the actin puncta precedes significant wound closure.

SCAR and Dia play distinct roles in actin assembly at wound edges

Having characterized the dynamics of the formation of actin puncta, cable, and protrusions at wound edges in wild-type embryos, we next used loss-of-function techniques to investigate the molecular mechanisms underlying their assembly. We focused our analysis on proteins known to promote actin filament formation or growth in other contexts.

First, we analyzed the effect of removing of zygotic expression of the Arp2/3 activator SCAR using the *SCAR*$^{\Delta 37}$ allele, which lacks all the protein-coding sequence of the *SCAR* gene (Zallen et al., 2002). We found that loss of zygotic *SCAR* dramatically reduced the formation of actin protrusions at the wound edge (Fig. 2, A and B). In contrast, there was little or no effect on the formation of the actin puncta or cable (Fig. 2, A and B; and Video 2). Consistent results were obtained when Sra1, a regulatory subunit of the SCAR complex (Eden et al., 2002; Kunda et al., 2003), was knocked down using RNAi (Fig. S1). Thus, we conclude that SCAR is a key regulator of actin protrusion formation at wound edges but plays little or no role in formation of the initial puncta or the actin cable, unless residual maternal SCAR is sufficient to form these structures. Surprisingly, loss of SCAR had only a minor effect on the speed of wound closure (Fig. 2 C). This suggests that either actin protrusions play a relatively small role in wound closure or that the embryo can effectively compensate for their loss (Wood et al., 2002; Abreu-Blanco et al., 2012).

To examine the role of Dia, we used *dia*^{5} maternal and zygotic mutant embryos (*dia*^{5} M/Z) in which Dia levels are greatly reduced (see Materials and methods; Homem and Peifer, 2008, 2009). In *dia*^{5} M/Z mutant embryos, formation of the wound edge actin cable was markedly inhibited, consistent with previous observations in the pupal epidermis (Antunes et al., 2013). Loss of Dia reduced protrusion levels, although less strongly than SCAR, and did not affect puncta formation (Fig. 3, A and B; and Video 3). Consistent results were obtained for offspring of *dia*^{5} germline clones crossed with males carrying a deficiency removing the *dia* gene (referred to as *dia*$^{5\,M}$/Df in Fig. 3 B; see also Materials and methods). To ensure that the loss of the actin cable in *dia*^{5} mutant embryos did not simply

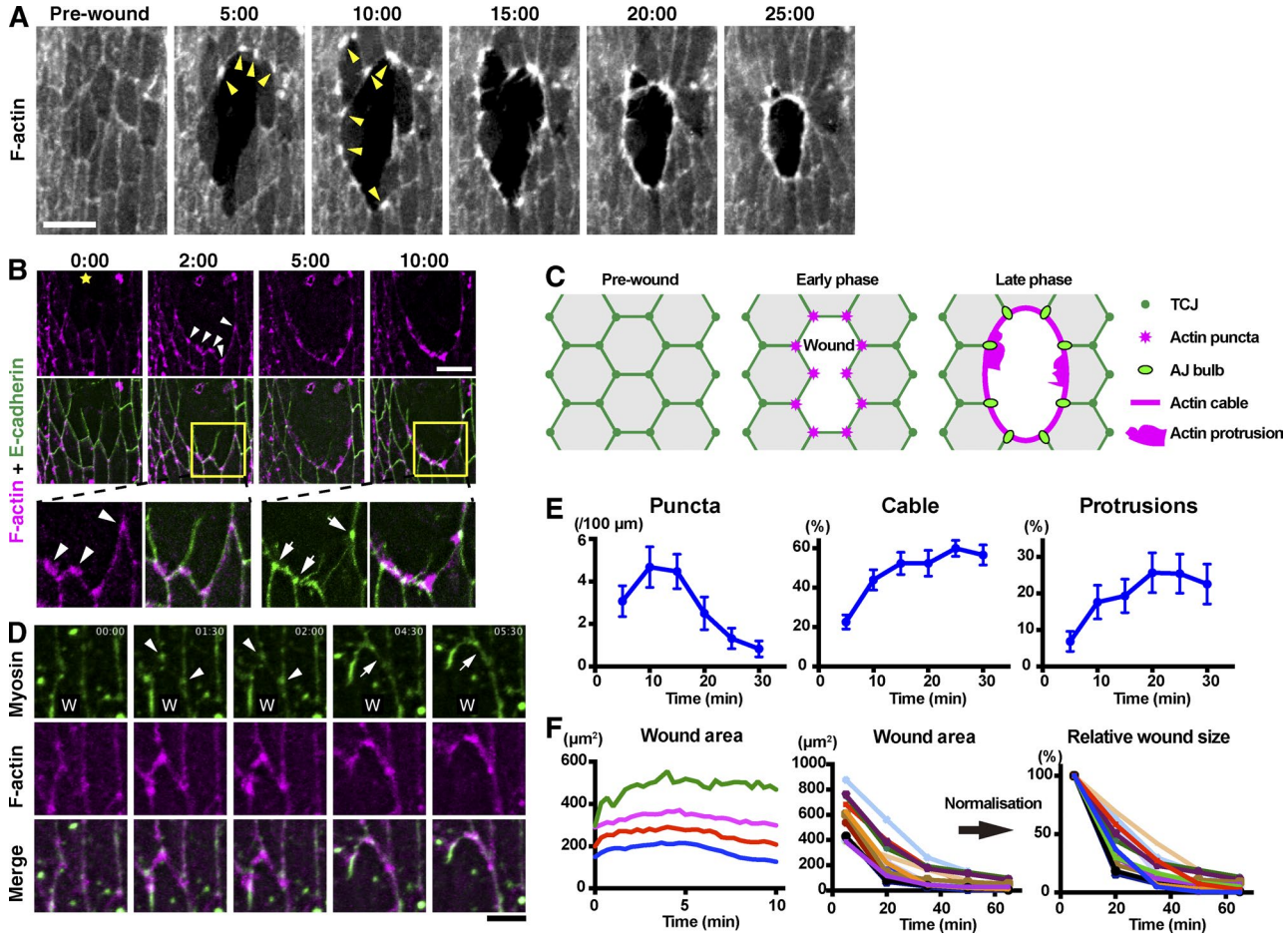

Figure 1. **Dynamics of F-actin, E-cadherin, and Myosin at wound edges.** (A) Time course of wound closure in *Drosophila* embryo expressing GFP-Moesin in the epidermis. Arrowheads indicate representative wound edge actin puncta. (B) The epidermis of a *Drosophila* embryo expressing the F-actin probe mCherry-Moesin (magenta) and E-cadherin–GFP (green) was wounded at the position marked by a yellow star and subjected to time-lapse live imaging. Bottom images show enlarged and enhanced images of the areas indicated by yellow squares in middle images. Arrowheads indicate actin puncta appearing at former-TCJs. Arrows indicate pronounced accumulations of E-cadherin where neighboring cells abut one another at the wound edge. (C) Cartoon illustrating the relationship between actin assembly and cell–cell junctions during wound healing. (D) Wound healing in an embryo expressing GFP-Zipper and mCherry-Moesin. W indicates position of wound. Arrowheads indicate myosin accumulations appearing and then enlarging at former-TCJs along the wound edge. Arrows indicate the formation of a link between two neighboring myosin accumulations. See also Video 1. (E) Wound closure was live imaged in embryos expressing GFP-Moesin and the prevalence of actin puncta, cable, and protrusions throughout the process was quantified as described in Materials and methods (graphs show means ± SEM; n = 10–15 embryos). (F) GFP-Moesin–expressing embryos were wounded, and wound area throughout closure was measured. (left) Wound area in first 10 min after wounding plotted against time at 20-s intervals. Data from four individual embryos are shown. The wounds expanded until ∼5 min and then began to reduce in area. (middle) Wound area throughout closure for 15 individual wounds of varying size measured at 15-min intervals until 65 min after wounding. Note that the wounds all close over a broadly consistent time course and with similar dynamics. (right) Data in middle graph were normalized against the area at 5 min. Time points indicate time after wounding (minutes and seconds) in A, B, and D. Bars: (A and B) 10 µm; (D) 5 µm.

reflect a global reduction in F-actin levels, we quantified the fluorescence intensity of wound edge F-actin and cortical F-actin just behind the wound edge at 4 min after wounding (Fig. S2 A). This revealed that in wild-type embryos, the intensity of wound edge actin is significantly greater than cortical actin behind, whereas in *dia*^{5} M/Z embryos, wound edge actin intensity is no greater than cortical actin behind (Fig. S2 B). This indicates that *dia*^{5} M/Z embryos fail in the de novo formation of F-actin at the wound edge and that the observed loss of actin at the wound edge in *dia*^{5} M/Z embryos does not merely reflect an overall reduction in F-actin levels.

Unexpectedly, in spite of the severe depletion of the wound edge actin cable, which is believed to be the main driver of wound closure (Wood et al., 2002; Abreu-Blanco et al., 2012), *dia*$^{5\,M}$/Df embryos closed wounds at a normal speed (Fig. 3 D). To investigate the mechanism by which wound closure occurs when Dia is depleted, we live-imaged GFP-Spaghetti-squash (myosin II light chain) in *dia*$^{5\,M}$/Df embryos. This revealed that myosin still accumulates at wound edges in *dia*$^{5\,M}$/Df embryos, although more slowly than in control embryos and in a patchy manner (Fig. 3 E). Close scrutiny of actin dynamics in *dia*^{5} M/Z embryos revealed that wound edge cells periodically formed diffuse assemblies of F-actin behind their edge. Formation of these structures correlated with a pulse of cell contraction (Fig. 3, A and C). This suggests when Dia is depleted and hence a continuous wound edge actin cable is not formed, wound closure can still proceed as a result of the formation of alternative contractile structures.

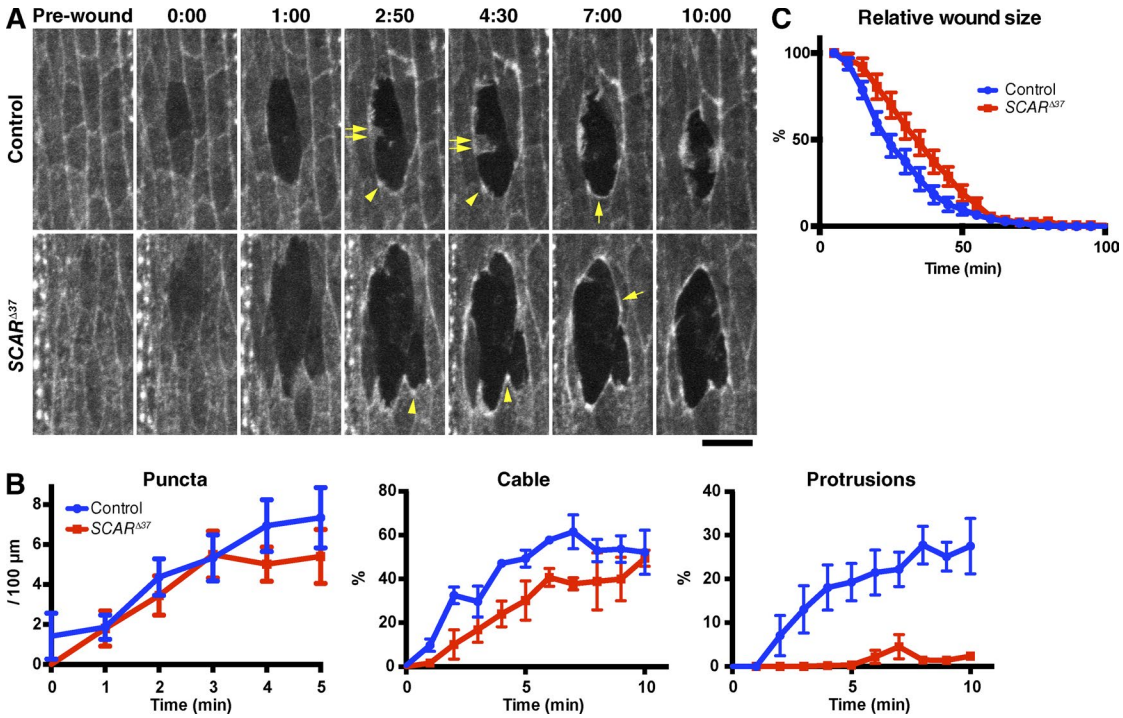

Figure 2. **SCAR function in actin remodeling at wound edges.** (A) Control and *SCAR*$^{\Delta 37}$ zygotic mutant embryos expressing GFP-Moesin were wounded and subjected to time-lapse imaging. Time points after wounding (minutes and seconds) are indicated. Note that although the actin puncta (arrowheads) and cable (single allows) appear in both the control and mutant embryos, the formation of actin protrusions (double allows) is severely reduced in the mutant, making its wound circumference markedly smoother than that of control. See also Video 2. Bar, 10 µm. (B) Quantitation of wound edge actin puncta, cable, and protrusion levels in control and zygotic *SCAR*$^{\Delta 37}$ embryos in the early phase of wound closure. n = 7–9 embryos. (C) Quantitation of wound closure in control and *SCAR*$^{\Delta 37}$ zygotic mutant embryos. Wound areas were normalized to the value at 5 min after wounding and plotted against time, as in Fig. 1 F. n = 4–17 embryos. Graphs show means ± SEM of the data.

WASp regulates the formation of actin puncta

As neither SCAR nor Dia mutant embryos showed defects in the formation of actin puncta, we reasoned that an alternative actin regulator must be responsible for these structures. We therefore examined the effect of loss of zygotic expression of WASp, using the *WASp*^{3} allele, which causes a frameshift and the loss of the C-terminal part of the WASp protein (Ben-Yaacov et al., 2001; Schäfer et al., 2007). Interestingly, loss of zygotic WASp caused a marked reduction in the formation of actin puncta at the wound edge (Fig. 4, A and B, left, P = 0.0005). Actin cable formation was unaffected by loss of zygotic WASp, whereas protrusion formation was reduced, albeit less severely than in *SCAR*$^{\Delta 37}$ embryos (Fig. 4, A and B, middle and right). The *WASp*^{3} mutation had little or no effect on the rate of wound closure (Fig. 4 C).

Dynamin localizes to actin puncta

Our finding that wound edge actin puncta are formed by a different nucleation pathway to the actin cable and protrusions suggests that rather than simply being the earliest part of the cable to form, the puncta are in fact distinct structures, potentially serving a distinct function. Several recent studies have identified WASp as a regulator of endocytosis, in particular endocytosis of AJs during junction remodeling (Georgiou et al., 2008; Leibfried et al., 2008). Given this role of WASp in AJ endocytosis and that the puncta mainly localize to specific cell junctions (former-TCJs), we hypothesized that the actin puncta may be sites of pronounced endocytosis and junction remodeling.

To test this hypothesis, we first analyzed the localization of the key endocytic regulator Dynamin during wound healing (Ferguson and De Camilli, 2012). We found that in the early stages of wound closure, Dynamin-GFP accumulates in spots at the wound edge, which colocalize with the actin puncta (Fig. 5 A and Video 4). Localization of Dynamin-GFP to the wound edge actin puncta is consistent with the hypothesis that these structures are sites of pronounced endocytosis. As wound closure proceeds, Dynamin-GFP puncta at the wound edge become more prevalent (Fig. 5 A). Dynamin-GFP accumulations at the wound edge remain punctate after actin distribution has become continuous as a result of the assembly of the actin cable (Fig. 5 A and Video 4).

Endocytosis is required for the actin remodeling during wound healing

To investigate the role of endocytosis in wound healing, we used *shibire*^{2} (*shi*^{2}), a temperature-sensitive allele of the gene encoding *Drosophila* Dynamin. We found that at the restrictive temperature of 30°C, *shi*^{2} embryos exhibited a marked defect in the formation of actin puncta, cable, and protrusions (Fig. 5, B and C). The absence of an actomyosin contractile cable in the mutant embryos was further confirmed by imaging GFP-Zipper (Fig. S3 A). Wound closure in *shi*^{2} embryos was significantly slower than in controls (Fig. 5 C, right). The reduction in closure speed in *shi*^{2} embryos was most pronounced in the first 15 min after wounding. After this time, the rate of closure was comparable with that of controls (Fig. 5 C). Ectopic expression of Dynamin-GFP rescued the defects wound closure and in the

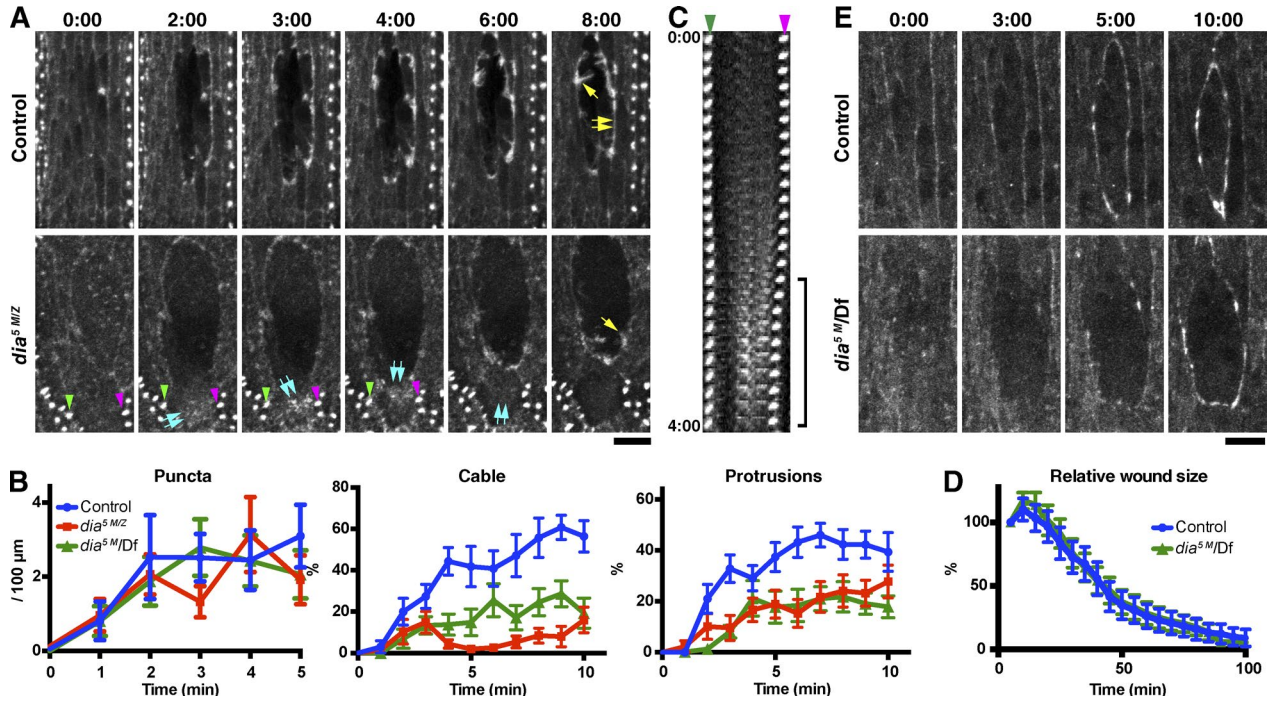

Figure 3. **Dia function in actin remodeling at wound edges.** (A) Time-lapse imaging of GFP-Moesin expressed in a control or *dia*^{5} M/Z embryo. Yellow single arrows indicate actin protrusions; yellow double arrows indicate actin cable. Blue double arrows in the *dia*^{5} M/Z images indicate diffuse assemblies of F-actin within a wound edge cell, which appear at 2 min, move upwards in the cell until 4 min and disappear by 6 min. See also Video 3. The denticles indicated by the green and magenta arrowheads in the *dia*^{5} M/Z images are visible in the kymograph in C. (B) Quantitation of wound edge actin puncta, cable, and protrusion levels in control, *dia*^{5} M/Z, and *dia*$^{5\,M}$/Df embryos in the early phase of wound closure. *n* = 9–13 embryos. (C) Kymograph analysis of the correlation between the formation of diffuse F-actin assemblies and cell contraction. The two denticles indicated by the green and magenta arrowheads in this panel and in A are equivalent. Note that the distance between the two denticles decreases when assemblies of F-actin (equivalent to blue double arrows in A) appear between them (bracket), consistent with this F-actin causing cell contraction. Images taken every 10 s until 4 min after wounding are shown. (D) Quantitation of wound closure in control and *dia*$^{5\,M}$/Df embryos. Wound areas were normalized to the value at 5 min after wounding and plotted against time. *n* = 3–13 embryos. (E) Time-lapse imaging of GFP-Spaghetti-squash expressed in a control (+/Df) or *dia*$^{5\,M}$/Df embryo. Time points indicate time after wounding (minutes and seconds). Graphs show means ± SEM of the data. Bars, 10 µm.

formation of all three actin structures caused by the *shi*^{2} mutation (Fig. 5, B and C). The *shi*^{2} mutation did not inhibit the formation of denticles on the ventral epidermis at the same developmental stage (Fig. S3 B), indicating that the wound edge actin assembly defects observed in *shi*^{2} embryos are not caused by a nonspecific perturbation of all actin-dependent processes or the death of the embryo. Collectively, these results indicate that Dynamin is essential for actin remodeling during wound healing and for efficient wound closure.

We also examined the dynamics of Clathrin, another key endocytic regulator, during wound healing. We observed punctate accumulations of Clathrin-GFP at the wound edge in wild-type embryos, whereas in *shi*^{2} mutants, no appreciable accumulation of Clathrin was observed at wound edges (Fig. 5 D). This observation is consistent with the notion that the wound edge is a location of pronounced Clathrin-mediated endocytosis, and this is disrupted in *shi* mutants.

Finally, to confirm that the defects observed in *shi*^{2} mutant embryos were caused by blockage of endocytosis, we also inhibited endocytosis by an alternative technique: expression of dominant-negative (DN) Rab5 (Rab5DN), which blocks the endocytic pathway by specifically perturbing the fusion of endocytic vesicles to early endosomes (Olkkonen and Stenmark, 1997; Entchev and González-Gaitán, 2002; Shimizu et al., 2003; Marois et al., 2006; Mateus et al., 2011). As observed for *shi*^{2}, Rab5DN blocked the formation of actin puncta, cable, and protrusions (Fig. 5 E and Videos 5 and 6) and reduced the speed of wound closure (Fig. 5 F). Collectively, these data strongly suggest that endocytosis plays a key role in regulating wound closure and the assembly of actin at wound edges.

Endocytosis is required for the recruitment of Dia to the wound edge

The observation that blocking endocytosis prevents wound edge actin assembly suggests that actin is misregulated in the absence of endocytosis. A possible reason for this is that recruitment of the appropriate actin regulators to the wound edge is dependent on endocytosis. To test this hypothesis, we examined the localization of Dia, the main nucleator of the actin cable, during wound healing in wild-type and *shi*^{2} embryos. We found that in wild-type embryos, GFP-Dia accumulated at the junctions between neighboring cells along the wound edge (Fig. 6 A, GFP-Dia, Control), colocalizing with the actin puncta (Fig. 6 B), whereas GFP alone did not accumulate at these junctions (Fig. 6 A, GFP). The proportion of wound edge junctions at which GFP-Dia accumulation was observed increased over the course of wound closure (Fig. 6 C). The mean intensity of GFP-Dia fluorescence at these junctions also increased over the course of closure and at 8 min after wounding is significantly greater than that of the equivalent TCJs before wounding ($P = 0.0404$), suggesting that GFP-Dia is newly recruited to these junctions after wounding (Fig. 6 D). In contrast, in *shi*^{2} embryos at the restrictive temperature, no accumulation of GFP-Dia was observed at the wound edge (Fig. 6, A, C, and D). This is con-

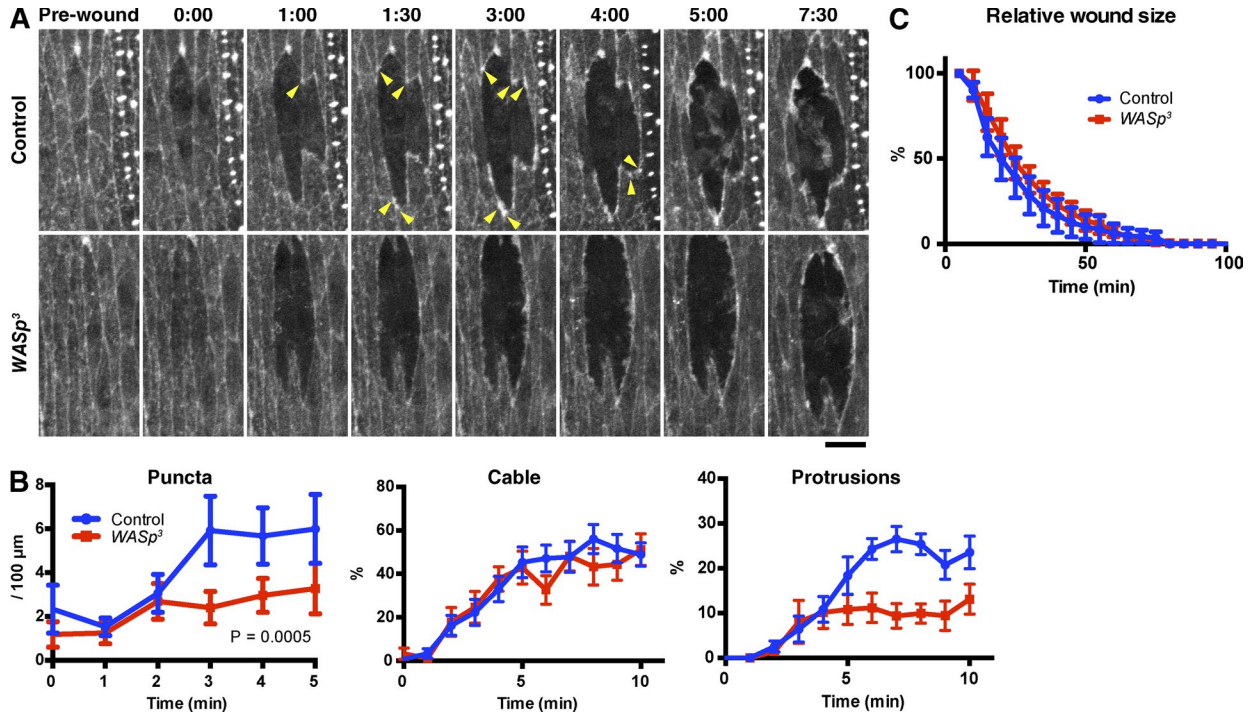

Figure 4. **WASp function in actin remodeling at wound edges.** (A) Time-lapse imaging of GFP-Moesin expressed in a control or *wasp*^{3} zygotic mutant embryo. Arrowheads indicate actin puncta. Time points indicate time after wounding (minutes and seconds). Bar, 10 µm. (B) Quantitation of wound edge actin puncta (left), cable (middle), and protrusions (right). *n* = 7–11 embryos. (C) Quantification of wound closure. Wound areas were normalized against the value at 5 min after wounding and plotted against time. *n* = 6–8 embryos. Graph show means ± SEM of the data.

sistent with the hypothesis that recruitment of actin regulators to the wound edge is dependent on endocytosis and suggests that the junctions between neighboring cells at the wound edge (corresponding to the former-TCJs in which actin puncta form) are important regulatory sites for actin assembly during wound healing. Consistent with previous observations (Homem and Peifer, 2009), we found that a constitutively active form of Dia lacking the C-terminal autoinhibitory domain (GFP-DiaΔ-DAD) localized more strongly than the full-length protein to cell–cell junctions, particularly TCJs, in intact epidermis (Fig. S5). Consequently, wounding did not induce an obvious redistribution of GFP-DiaΔDAD (Fig. S4). These data suggest that localization of Dia to cell–cell junctions is increased when it is in an activated state, so the observed recruitment of Dia to wound edge junctions may indicate that it is specifically activated at these sites after wounding.

Endocytic regulation of wound edge actin assembly involves AJ remodeling

Remodeling of AJs is essential during epithelial morphogenesis, and this remodeling is driven by the endocytosis and recycling of junction components (Harris, 2012). Given the many similarities between epithelial morphogenesis and repair (Martin and Parkhurst, 2004; Matsubayashi and Millard, 2013), we hypothesized that endocytosis-dependent remodeling of AJs is likely to also play important roles in wound healing, thus providing a possible explanation for the defective wound response observed on blocking endocytosis. To test this hypothesis, we first examined whether the remodeling of wound edge AJs to form "bulbs" at wound edge (Figs. 1 B and 7 A; Wood et al., 2002) is dependent on endocytosis. We found that in wild-type embryos the majority of wound edge AJs acquired the distinctive bulb-like morphology in the minutes after wounding (Fig. 7, A and B). In contrast, in Rab5DN-expressing embryos, wound edge AJs rarely underwent obvious bulb formation, demonstrating that this wound-induced remodeling of the AJ requires endocytosis (Fig. 7, A and B). Then, we tested whether AJs are important for wound healing, using a mutant of the gene encoding *Drosophila* E-cadherin, *shotgun* (*shg*). We found that homozygous zygotic *shg*^{k03401} mutant embryos exhibited a marked delay in wound closure (Fig. 7, C and D, left). The formation of actin cable and protrusions were significantly impaired by zygotic loss of *shg* expression, although puncta formation was not. These results demonstrate that AJs play an essential role in wound healing and wound edge actin assembly; therefore, the remodeling that they undergo after wounding is likely to be important for these processes. Finally, we tested for genetic interactions between *shi*^{2} and genes encoding AJ components. We reasoned that if *shi*^{2} disrupts wound healing because it compromises the function of AJs in the process, perturbing junctions further should enhance *shi*^{2} phenotypes. Experiments were performed at 25°C, a temperature at which Dynamin function is reduced but not completely eliminated in *shi*^{2} embryos. Crucially for our analysis, at this temperature, *shi*^{2} mutants heal wounds at the same speed as wild-type embryos. To partially disrupt AJ function, we removed one copy of *shg* (*shg*^{k03401}/+). In isolation, loss of one copy of *shg* did not affect wound closure speed. However, the combination of *shg*^{k03401}/+ with *shi*^{2} at 25°C resulted in a significant slowing of wound closure (Fig. 7 E, left). We then examined the effect of partial loss of *shg* on wound edge actin assembly. Mutation of a single copy of the *shg* gene in a wild-type background did not affect the formation of actin

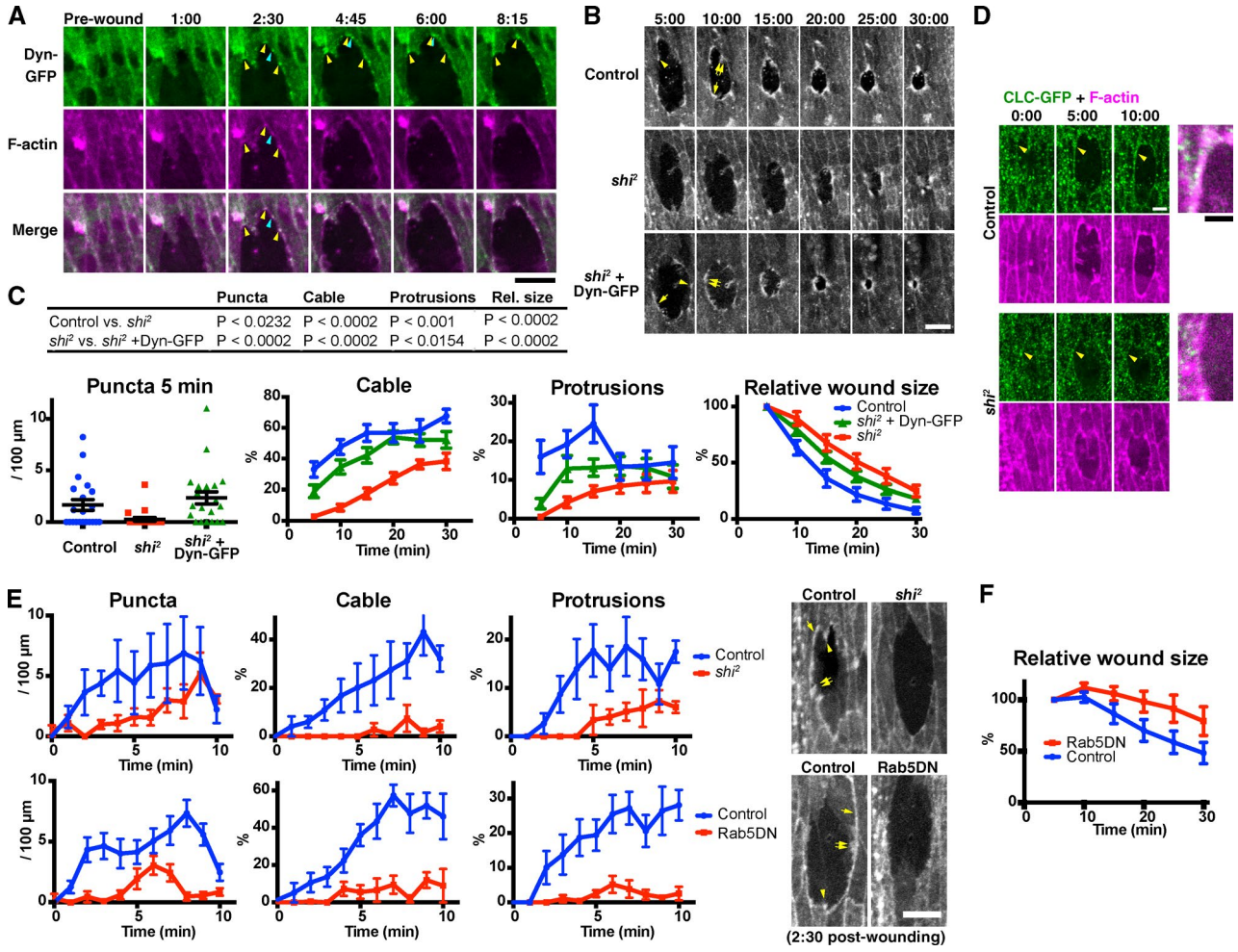

Figure 5. **Endocytosis is required for wound edge actin remodeling and wound closure.** (A) Time-lapse live imaging of an embryo expressing Dynamin-GFP (Dyn-GFP, green) and mCherry-Moesin (magenta). At 2 min and 30 s, Dynamin-GFP and F-actin colocalize at puncta on the wound edge, at (yellow arrowheads) and also outside (blue arrowheads) former-TCJs. The Dynamin-GFP puncta at former-TCJs were relatively stable and stationary, whereas those at other sites were more transient and mobile. See also Video 4. (B) Time-lapse live imaging of mCherry-Moesin, expressed in control and *shi²* embryos (top and middle rows, respectively), and a *shi²* embryo expressing Dynamin-GFP (*shi²* + Dyn-GFP, bottom row). Representative actin puncta (arrowheads), cables (single arrows), and protrusions (double arrows) are indicated. (C) Quantitation of wound edge actin puncta, cable, protrusions, and wound closure (left to right, respectively) in control embryos, *shi²* embryos, and *shi²* embryos expressing Dynamin-GFP. Note that puncta were quantified only at 5 min because at later time points, they are obscured by the actin cable and protrusions (see also Fig. 1). *n* = 12–21 embryos (actin puncta, cable, and protrusions) or 15–16 (wound closure). For the measurement of wound closure, wound area was normalized against the value at 5 min after wounding. The table at the top summarizes the results of statistical analyses of the data. (D) Time-lapse live imaging of a control or *shi²* mutant embryo expressing Clathrin light chain-GFP (CLC-GFP; green) and mCherry-Moesin (magenta). Merged images at the right show the wound edge around the arrowheads in the 10:00 images. Note the punctate accumulations of Clathrin-GFP at the wound edge in the control but not in *shi²* embryos (arrowheads). (E, top) A more detailed analysis of the formation of actin structures in control or *shi²* embryos in the early phase of wound closure. Here, F-actin was visualized using GFP-Moesin. The results confirm the actin remodeling defects observed for *shi²* embryos in the longer term analysis in B and C. *n* = 3–4 embryos. (bottom) Quantitation of actin puncta, cable, and protrusions in control or Rab5DN-expressing embryos. F-actin was visualized using GFP-Moesin. *n* = 6–8 embryos. Photographs at the right are representative images at 2 min and 30 s after wounding, of the embryos of indicated genotype. See also Videos 5 and 6. (F) Quantitation of wound closure control or Rab5DN-expressing embryos, performed as in C, rightmost graph. *n* = 10–11. Time points indicate time after wounding (minutes and seconds). Bars, 10 µm. All experiments involving *shi²* were performed at 30°C, the restrictive temperature of this mutant. Bars in column scatter plot (C, left) indicate means ± SEM of all plotted values. Line graphs in C, E, and F show means ± SEM of the data.

puncta, cable, or protrusions during wound healing. However, loss of one copy of *shg* significantly enhanced the defect in actin cable formation resulting from partial loss of Dynamin activity (*shi²* at 25°C; Fig. 7 E, Cable). The same trend was observed for actin protrusions, although statistical significance was not detected (Fig. 7 E, Protrusions). The effect of *shg* mutation on actin puncta could not be analyzed because *shi²* alone almost completely blocked the puncta formation at 5 min (Fig. 7 E, rightmost graph).

We also examined the genetic interaction of *shi²* with a second AJ component, p120-catenin (p120ctn; Myster et al., 2003). In *Drosophila*, p120ctn is not essential for AJ function but instead plays a supporting role (Myster et al., 2003). We depleted both maternal and zygotic p120ctn from wild-type embryos and found that this did not affect the speed of wound closure (Fig. 7 F, left-hand graph). However, the combination of p120ctn depletion with *shi²* at 25°C resulted in a significant slowing of wound closure (Fig. 7 F, second graph from the left). Moreover, the depletion of p120ctn from *shi²* mutant embryos significantly enhanced the defect in the formation of both actin cable and protrusions in *shi²* mutant embryos (Fig. 7 F, green triangles vs. magenta inverted triangles). Collectively, the ge-

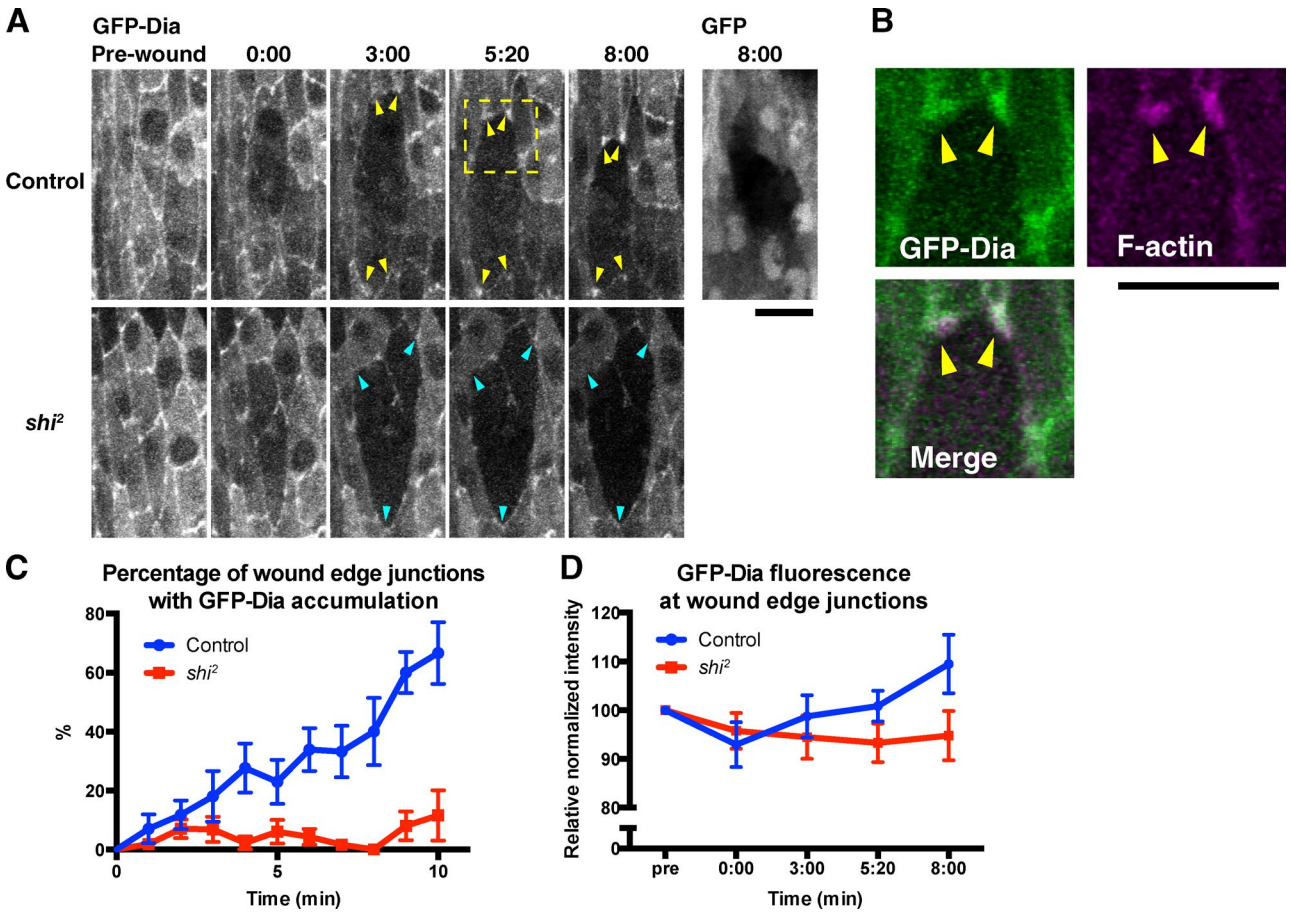

Figure 6. **Dynamin-dependent relocalization of Dia during wound healing.** (A, top) Time-lapse live imaging of embryos expressing GFP-Dia or GFP together with mCherry-Moesin in wild-type embryos. Note that GFP-Dia is recruited to wound edge junctions after wounding (arrowheads), whereas GFP alone is not (rightmost image). (bottom) Behavior of GFP-Dia in a wounded *shi²* embryo. Note that the fluorescence level at wound edge junctions does not increase (arrowheads). Time points indicate time after wounding (minutes and seconds). (B) The enlarged images of GFP-Dia (green) and mCherry-Moesin (magenta) in the area indicated by the dashed square in A (Control, 8:20). Note the colocalization of GFP-Dia and actin puncta (arrowheads). (C and D) Dia accumulation over the course of wound healing in wild-type and *shi²* embryos, measured in two distinct ways as described in Materials and methods. (C) Semiquantification based on the size and brightness of GFP-Dia accumulation at wound edge junctions. *n* = 5–7 embryos. Each image contained 3–23 wound edge junctions. (D) Quantification of the GFP-Dia fluorescence intensity at wound edge junctions. *n* = 27–31. Note that in both C and D, the value indicating the accumulation of GFP-Dia increases after wounding in control but not *shi²* embryos. All experiments were performed at 30°C. Graphs show means ± SEM of the data. Bars, 10 µm.

netic interaction of Dynamin with two distinct AJ components, E-cadherin and p120ctn, support the hypothesis that endocytic remodeling of AJs is required for actin assembly at wound edges and for wound closure.

Evolutionary conservation of the role of Dynamin in wound edge actin remodeling

We then examined whether endocytosis is also involved in actin remodeling during wound healing by mammalian epithelial cells. When a confluent monolayer of mIMCD3 mouse kidney epithelial cells (Rauchman et al., 1993) is scratch wounded, an actomyosin cable and actin protrusions form at the wound edge, as shown by staining for F-actin and activated nonmuscle myosin II (Fig. 8 A). Thus, as for MDCK and caco-2 cells, this cell line can be used as an in vitro model to study actin remodeling during epithelial wound healing (Bement et al., 1993; Fenteany et al., 2000). Dynasore, a chemical inhibitor of Dynamin, was applied to monolayers before scratch wounding to inhibit endocytosis (Macia et al., 2006). As observed in *Drosophila* embryos, formation of actin cable and protrusion at the wound edge were strongly inhibited by dynasore (Fig. 8, A and B). Moreover, dynasore also inhibited the migration of the wound edges across the scratch wound (Fig. 8, C and D). Staining with an anti-Clathrin antibody revealed punctate accumulations of Clathrin in the vicinity of actin assemblies at the wound edge of untreated monolayers; however, these Clathrin accumulations were absent in dynasore-treated monolayers (Fig. 8 E). This suggests that wound edges are sites of pronounced Dynamin-dependent, Clathrin-mediated endocytosis in scratched mIMCD3 monolayers. These results are consistent with those we obtained for *Drosophila* (Fig. 5) and suggest that the roles of Dynamin and endocytosis in wound closure are evolutionarily conserved.

Discussion

Our research shows that several different actin regulators contribute to the assembly of actin filaments at wound edges. Absence of Dia results in a severe depletion of the actin cable that encircles the wound, suggesting that Dia is the predominant

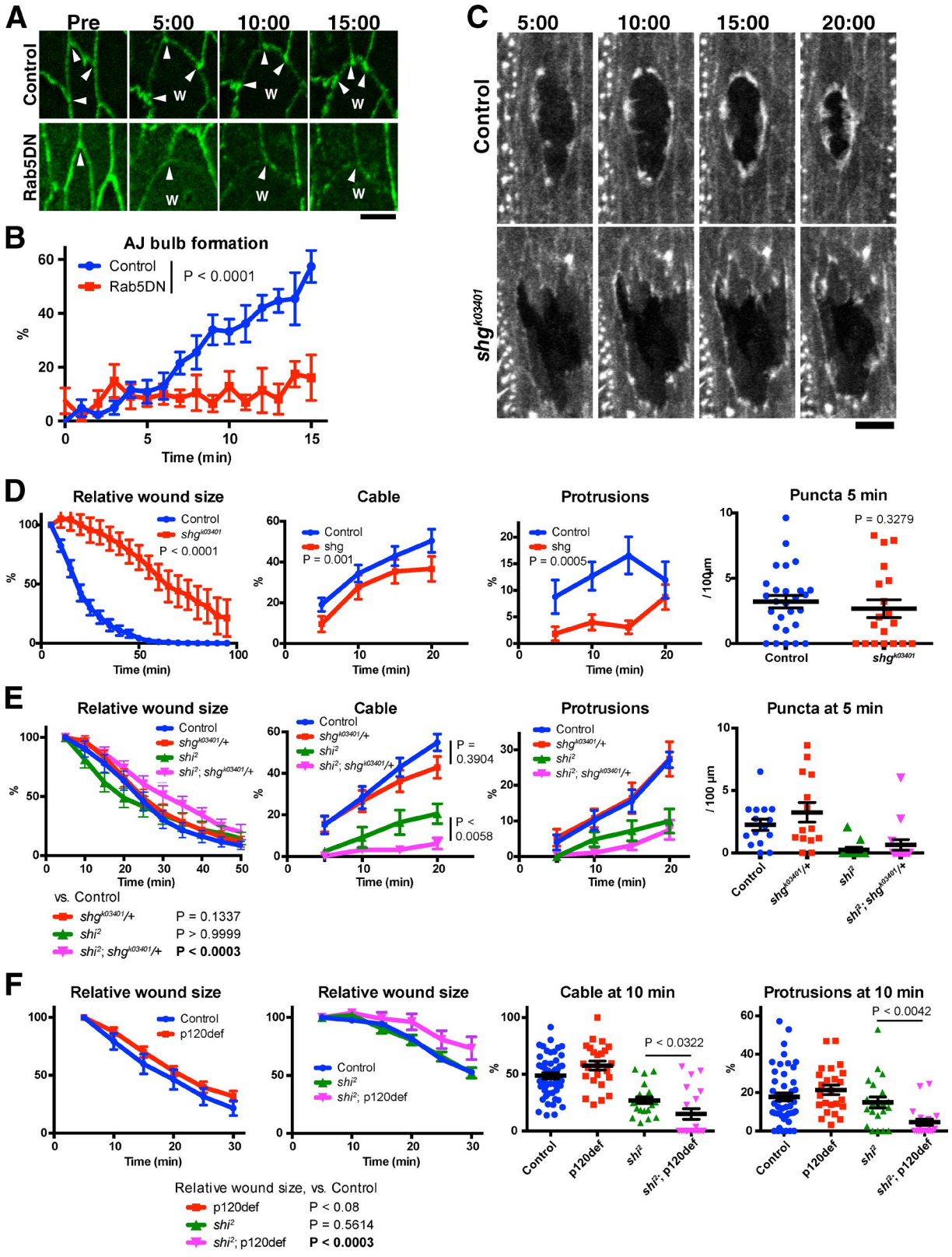

Figure 7. **Genetic interactions between Dynamin and AJ components.** (A and B) Effect of Rab5DN on the formation of wound edge AJ bulbs. (A) Representative images of control and Rab5DN-expressing embryos prewounding (Pre) and at the indicated time points after wounding. Note the presence (control) and absence (Rab5DN) of AJ bulbs at wound edge (arrowheads). The images of Rab5DN embryos were enhanced to highlight the shape of wound edge junctions. W indicates position of wound. (B) Quantification of AJ bulb formation over the course of wound healing in control and Rab5DN-expressing embryos, measured as described in Materials and methods. *n* = 6 or 7 embryos. Each image contained 3–23 wound edge junctions. (C and D) Analysis of the wound healing of zygotic homozygous *shg* mutant embryos. (C) Representative images of F-actin visualized using GFP-Moesin in embryos with indicated genotype at indicated time points. (D) Normalized wound area and the formation of actin puncta, cable, and protrusions in embryos of the indicated

nucleator of the actin filaments that form this structure. Several studies have concluded that the wound edge actin cable is the main driver of wound closure in *Drosophila* embryos (Wood et al., 2002; Abreu-Blanco et al., 2012); therefore, it was surprising that closure speed was unaffected in *dia* mutants. This discrepancy may be caused by the fact that in these previous studies, Myosin II, the motor component of the cable, or its regulator Rho were disrupted rather than the assembly of actin filaments. Notably, we find that Myosin II still accumulates at the wound edge in *dia* mutants, albeit slowly and more irregularly. This suggests that in the absence of Dia, ad hoc contractile actomyosin structures are assembled at the wound edge, perhaps using preexisting cortical actin, or actin filaments nucleated by the Arp2/3 complex. We conclude that although recruitment of Myosin II to the wound edge is necessary for efficient wound closure, formation of a continuous, well-defined actin cable is not. Therefore, our experiments involving Dia loss of function suggest that the quantity of F-actin in the wound edge actin cable is not a major determinant of the rate of the wound closure. In contrast to actin cable assembly, the formation of actin protrusions is strongly dependent on the activity of the Arp2/3 complex activator SCAR. Loss of SCAR activity almost entirely eliminated protrusive activity. This only had a modest effect on wound closure speed, which was surprising as previous studies have proposed a more significant role for protrusions in *Drosophila* wound closure (Wood et al., 2002; Abreu-Blanco et al., 2012). This difference may be caused by the fact that these previous studies eliminated protrusions by inactivating Cdc42. Besides promoting actin protrusion formation, Cdc42 has other important roles, including regulation of AJ endocytosis (Georgiou et al., 2008; Leibfried et al., 2008). Therefore, it is possible that wound phenotypes observed on disruption of Cdc42 are not solely caused by loss of wound edge protrusions. Overall, our analysis of Dia and SCAR loss of function reveals wound closure in *Drosophila* embryos to be more robust and adaptable than previously realized. It would be interesting to determine whether loss of both Dia and SCAR would result in a more severe disruption of wound closure, but unfortunately, this experiment was not possible for technical reasons (see Materials and methods).

Our analysis revealed that formation of the actin cable and protrusions at wound edges was preceded by the assembly of punctate actin structures. Unlike the cable and protrusions, these actin puncta were not affected by loss of Dia or SCAR. Our data show that instead WASp is responsible for their formation. This difference in nucleation mechanisms suggests that these puncta are in fact distinct structures, rather than simply being the first part of the actin cable to assemble. Several studies have shown that WASp participates in the remodeling of AJs in *Drosophila* epithelia by generating actin filaments that promote endocytosis of AJ components, raising the possibility that the puncta could be sites of AJ endocytosis (Georgiou et al., 2008; Leibfried et al., 2008). Consistent with this idea, GFP-fused Dynamin, a key endocytosis regulator (Ferguson and De Camilli, 2012), colocalizes with the actin puncta. Blocking endocytosis strongly inhibits all actin assembly at the wound edge, indicating that endocytosis is critical for wound responses and acts upstream of actin regulators. Genetic interaction of *shi*/dynamin with both *shg*/E-cadherin and *p120ctn* supports the notion that the defects in wound edge actin assembly and wound closure observed on blocking endocytosis are at least in part a result of a failure in AJ remodeling. If the observed WASp-dependent actin assembly at wound edges is involved in AJ endocytosis, we might expect wound closure to be disrupted in *WASp* mutant embryos, as we observe in *shi* mutants; however, wound closure was unaffected in *WASp* mutants. A possible explanation for this result is that there is an alternative mechanism for AJ endocytosis that doesn't require WASp, and this alternative mechanism can compensate when WASp is absent. Consistent with this hypothesis, a previous study showed that AJ endocytosis is only partially disrupted in *WASp* mutants (Georgiou et al., 2008).

The wound edge actin puncta discussed in the previous paragraph predominantly form at sites that were TCJs before wounding. These sites appear to play a central role in wound responses and undergo a series of changes as wound closure proceeds (illustrated in Fig. 1 C). After wounding, these former-TCJs are the first sites on the wound edge at which actin, myosin, and Dynamin accumulate. The majority of the former-TCJ sites then become the junctions that link neighboring wound edge cells and recruit Dia, the main nucleator of the actin cable. Previously, we have shown that phosphatidylinositol 3,4,5-trisphosphate, a signal that promotes actin protrusion formation, also accumulates at these junctions (Pickering et al., 2013). This suggests that these wound edge junctions may be "signaling centers" that coordinate wound edge actin and myosin dynamics. These wound edge junctions also enlarge to become the bulb-like AJs that link the actin cable from cell to cell (Danjo and Gipson, 1998; Wood et al., 2002). Collectively, these findings suggest that after wounding, TCJs are remodeled to become specialized signaling/support structures for wound healing. Notably, the enlargement of AJs at the wound edge and their recruitment of Dia both require endocytosis, suggesting that the formation of these structures is accomplished by endocytic remodeling. This likely explains why endocytic activity appears to be particularly high at former-TCJ sites. Notably, Dynamin-GFP remains at former-TCJs even after wound edge actin has become continuous as a result of assembly of the actin cable, suggesting that endocytosis at former-TCJs is important throughout healing, not just for the initiation of actin remodeling. Our finding that wound closure is slowed and wound edge actin assembly is reduced in zygotic *shg* mutant embryos supports the notion that AJs play a central role in regulating and driving wound closure. One unexpected finding is that the formation of actin puncta is unaffected in this mutant; however, it is possible that residual maternally contributed E-cadherin is sufficient for these structures to form. A recent study showed that disruption of the Toll–NF-κB pathway prevented remodeling of AJs and actin after wounding of *Drosophila* embryos,

genotypes were quantified and plotted (left to right, respectively). *n* = 5–27 embryos. (E) Analysis of the effect on wound closure and wound edge actin remodeling of loss of one copy of *shg* in a wild-type (control) or shi^2 background. Normalized wound area and the formation of actin puncta, cable, and protrusions in embryos of the indicated genotypes were quantified and plotted (left to right, respectively). *n* = 8–22 embryos. (F) Analysis of the effect on wound closure (left two graphs, *n* = 15–20), and wound edge actin remodeling (right two graphs) of loss of both maternal and zygotic p120ctn (p120def) from wild-type (control) or shi^2 embryos. Normalized wound area and the formation of actin cable and protrusions in embryos of the indicated genotypes were quantified and plotted. All experiments were performed at 25°C. Time points indicate time after wounding (minutes and seconds). Bars indicate the means ± SEM of all plotted values. Bars: (A) 5 µm; (C) 10 µm.

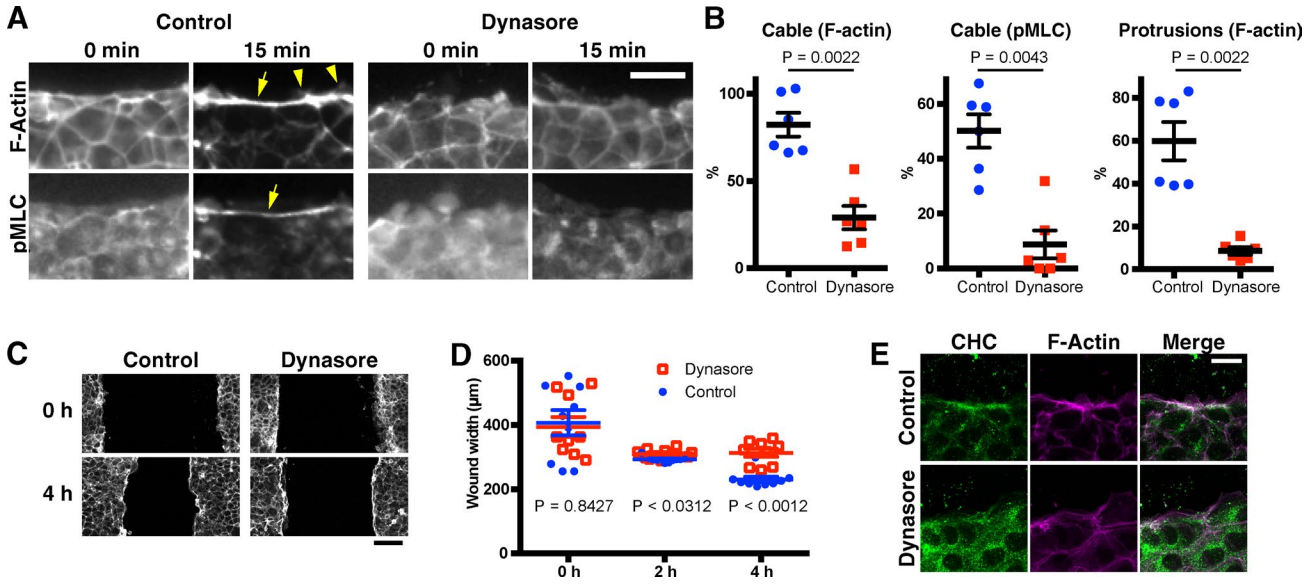

Figure 8. **Dynasore inhibits wound edge actin remodeling by mammalian cells.** Confluent monolayers of mIMCD3 mouse kidney epithelial cells were scratch wounded after treatment with DMSO (control) or 80 µM dynasore, a chemical inhibitor of Dynamin. At the indicated time points, the cells were fixed and stained with rhodamine-phalloidin and antibodies against phospho (=activated) myosin light chain (pMLC) or clathrin heavy chain (CHC), to examine the formation of an actomyosin cable and actin protrusions at the wound edge and the intracellular localization of clathrin. (A) Representative phalloidin and anti-pMLC images of control and dynasore-treated cells at 0 and 15 min after wounding. Arrows and arrowheads indicate the actin (myosin) cable and protrusions, respectively. (B) Cable and protrusion formation in the images 15 min after wounding was quantified. Cable formation was quantified using both the F-actin and pMLC images. Protrusions were quantified using the F-actin images. Note that the formation of both actin cable and protrusions are inhibited by dynasore. (C) Low magnification phalloidin images at 0 and 4 h after wounding. Note that the advancement of the cell sheets is inhibited by dynasore. At 4 h, a wound edge actin cable is observed, even for dynasore-treated cell sheets. (D) Quantification of wound width in each sample at the indicated time points. (E) Representative phalloidin and anti–clathrin heavy chain images of control and dynasore-treated cells at 15 min after wounding. Bars in the column scatter plots indicate means ± SEM of all plotted values. Line graphs show means ± SEM of the data. Bars: (A and E) 20 µm; (C) 100 µm.

suggesting that this pathway is part of the signaling mechanism that triggers AJ remodeling in response to tissue damage (Carvalho et al., 2014).

TCJs are defined structures with a different complement of resident proteins to normal "bicellular" junctions (Schulte et al., 2003; Ikenouchi et al., 2005; Lye et al., 2014). It is possible that this difference in composition primes these sites for rapid activation of actin assembly and/or endocytosis when a wound is sustained. In addition, it has been recently reported that mammalian TCJs play crucial roles in the regulation of actomyosin activity through the Cdc42 activator Tuba (Oda et al., 2014). Cdc42 acts upstream of WASp and Dynamin in the endocytosis of E-cadherin (Salazar et al., 2003; Georgiou et al., 2008; Leibfried et al., 2008), providing a potential mechanistic link between TCJs, actin assembly, and AJ remodeling. What triggers actin assembly and endocytosis to commence at former-TCJs when a wound is sustained? One possibility is that TCJs are responding to changes in mechanical tension resulting from wounding. In the *Drosophila* embryonic epidermis, circumferential actomyosin fibers produce tension along cell edges that is balanced at TCJs (Kiehart et al., 2000; Ishihara and Sugimura, 2012). TCJs are therefore well placed to detect changes in tissue tension after wounding and implement wound closure mechanisms in response.

Our analysis focused on the role of endocytosis in wound edge actin assembly and AJ remodeling; however, it is likely that endocytosis also contributes to wound healing by other mechanisms. For instance, it has recently been demonstrated that wound closure in *Drosophila* embryos involves cell rearrangements behind the wound edge, which are similar to those that occur during germband extension (Levayer et al., 2011; Razzell et al., 2014). Because germband extension cell rearrangements require the endocytosis-dependent remodeling of AJs, it is likely that those occurring during wound healing also do. In addition, receptor tyrosine kinase signaling is influenced by receptor trafficking, both positively and negatively (Miaczynska et al., 2004; Sadowski et al., 2009). At least two receptor tyrosine kinases, Stitcher and the EGF receptor, participate in *Drosophila* embryonic wound closure and are therefore potentially important targets of endocytosis (Wang et al., 2009; Geiger et al., 2011).

In summary, our data reveal that actin assembly at wound edges requires the coordination of a variety of different actin regulators, each of which makes a distinct contribution to the process. In addition, endocytosis plays an important and hitherto unknown role in triggering actin assembly at wound edges. We conclude that complex interplay between actin assembly, AJ remodeling, and membrane traffic is required for the construction of a motile leading edge during wound healing. Our finding that dynasore, a chemical inhibitor of Dynamin, impaired wound closure and wound edge actin assembly during healing of scratch wounds in mammalian epithelial cultures suggests that the interplay between endocytosis and actin remodeling during wound healing may be conserved across diverse species and tissues and could therefore be of medical significance.

Materials and methods

Fly stocks

w^{1118} were used as wild-type controls. The following transgenic strains harboring probes for F-actin were used: constitutive GFP-Moesin (Kie-

hart et al., 2000), UAS-GFP-Moesin (Dutta et al., 2002), and UAS-mCherry-Moesin (Millard and Martin, 2008). The other transgenic lines used are as follows: UAS-*ebony (e)* RNAi (28612; Bloomington Stock Center), UAS-*sra1* RNAi (38294; Bloomington Stock Center), UAS-Rab5DN (Entchev and González-Gaitán, 2002), UAS-RedStinger (8547; Bloomington Stock Center), UAS-GFP-Zipper (Franke et al., 2005), UAS-GFP-Dia, UAS-GFP-DiaΔDAD (Homem and Peifer, 2009), UAS-GFP (5430; Bloomington Stock Center), UAS-Dynamin-GFP (Rikhy et al., 2015), UAS–clathrin light chain (7107; Bloomington Stock Center), Sqh-GFP expressed under the control of the *sqh* promoter (42235; Bloomington Stock Center), and ubiquitin–E-cadherin–GFP (Oda and Tsukita, 2001). TubP-Gal4 (Lee and Luo, 1999) was used to express transgenes ubiquitously. e22c-Gal4 (Jacinto et al., 2000), i76d-Gal4 (Kyoto stock 106535; Drosophila Genomics Resource Center), and 112A-Gal4 (7021; Bloomington Stock Center) were used to express transgenes throughout the epidermis. The following mutant alleles and deficiencies were used: $SCAR^{\Delta 37}$ (Zallen et al., 2002), $WASp^{3}$ (39725; Bloomington Stock Center), dia^{5} (9138, also harboring P{neoFRT}40A; Bloomington Stock Center; Homem and Peifer, 2008), Df(2L)ED1317 (a chromosomal deficiency removing genes including *dia*; 9175; Bloomington Stock Center), shi^{2} (temperature sensitive; Kim and Wu, 1990), shg^{k03401} (10377; Bloomington Stock Center), $p120ctn^{308}$ (null but homozygous viable and fertile; 6664; Bloomington Stock Center; Myster et al., 2003), and Df(2R)M41A10 (a chromosomal deficiency removing genes including *p120ctn*; 741; Bloomington Stock Center). The shi^{2} and $p120ctn^{308}$ mutant flies were maintained as homozygous stocks. The other mutants and deficiencies were maintained as heterozygous stocks with an appropriate balancer. Flies carrying more than one of the mutations and transgenes listed in this paragraph were obtained by crossing and recombination. Balancer chromosomes expressing fluorescent proteins were used to identify embryos of appropriate genotype. The genotypes of the embryos used in each experiment are summarized in Table S1. To carry out the loss-of-function experiments of Dia while circumventing the oogenesis and cellularization defects caused by the complete depletion of maternal Dia (Afshar et al., 2000; Homem and Peifer, 2008), we took the approach used by Homem and Peifer (2009). First, germline clones of dia^{5}, whose maternal Dia protein is greatly reduced but not completely depleted, were generated using the FLP-dominant female sterile technique (Chou and Perrimon, 1996). Female flies bearing the clones were crossed with males carrying dia^{5} or Df(2L)ED1317, and the resulting embryos were incubated at 18°C until stage 15. The fact that germline clones were required to observe *dia* loss-of-function phenotypes precluded the possibility of studying the effect of loss of *dia* and *SCAR* in combination because the two genes reside on the same chromosome arm and germline clones of *SCAR* loss-of-function mutants do not produce viable oocytes (Zallen et al., 2002). p120ctn-deficient embryos were generated by crossing $p120ctn^{308}$/Df(2R)M41A10 females to males homozygous for $p120ctn^{308}$.

Preparation of *Drosophila* embryos for live imaging

Flies were left to lay eggs at 18°C for 1–2 d or at 25°C overnight on apple juice agar. Embryos were collected and dechorionated in 50% bleach. Those at stage ∼15 were selected and mounted in a 3:1 mix of halocarbon oils 700 and 27 (Sigma-Aldrich) between a glass coverslip covered with or without heptane glue (Brust-Mascher and Scholey, 2009) and a gas-permeable Lumox culture dish (Greiner) as described previously (Evans et al., 2010; Pickering et al., 2013).

Confocal microscopy and image processing

Images of *Drosophila* embryos were acquired using a confocal microscope (60× NA 1.4 CFI-Plan Apochromat oil objective; A1R; Nikon) and NIS-Elements software (Nikon). All imaging was performed at 25°C unless otherwise stated. Laser wounding was performed using an ablation laser (MicroPoint; Andor Technology) attached to the Nikon microscope, to the ventral epidermis of embryos. For time-lapse imaging with 5 min or longer time intervals, ≤21 embryos were simultaneously observed using the multipoint-imaging mode of the microscope. In this case, because multiple embryos needed to be wounded before starting imaging, the first frames of the data were taken 5 min after wounding. Acquired images were processed and analyzed with ImageJ (National Institutes of Health). Maximum projection images were made from Z stacks and used for analyses and presentation. If background autofluorescence from embryos perturbed observation of expressed fluorescent probes, the background fluorescence was removed before making maximum projection images, using a median filter-based method (Wu et al., 2010). In brief, using ImageJ, original Z-stack images were first processed with a median filter, whose radius was empirically set to 15 pixels. Then, the filtered images were subtracted from the originals, to produce background-removed images. This technique was used to obtain the data in Figs. 1 (B and D) and 7 A. In addition to ImageJ, Photoshop and Illustrator (Adobe) were used for image contrasting and compilation.

Cell culture, scratch wound assay, and immunocytochemistry

mIMCD3 cells (subclone C11; Matsubayashi et al., 2011) were cultured in DMEM/F12 (Invitrogen) supplemented with 10% fetal calf serum and antibiotics (100 U/ml penicillin, 100 µg/ml streptomycin, and 20 µg/ml kanamycin; Shaw and Martin, 2009). Cells were split onto glass coverslips in 24-well plates at the density of 10^{5} cells/well 3 d before and replenished with fresh medium 1 d before wounding. Dynasore (EMD Millipore) was diluted to 100 mM stock in DMSO. Cells were incubated in fresh culture medium containing control DMSO (0.24% vol/vol) or final 80 µM dynasore for 30 min before wounding. In the continuous presence of the drug, the cell sheets were scratch wounded with a pipette tip and fixed 0 and 15 min after wounding with 4% formaldehyde in PBS (room temperature 15 min). After being washed with PBS, the cells were incubated overnight with rabbit anti–phospho-myosin light chain 2 (Ser19) antibody (dilution 1:50; Cell Signaling Technology) or mouse anti–clathrin heavy chain antibody (dilution 1:1,000; Merck) in the blocking solution (PBS containing 3% BSA and 0.5% Triton X-100) at 4°C. Then, the cells were washed with PBS and incubated with the blocking solution containing an appropriate secondary antibody (FITC-conjugated anti–rabbit, dilution 1:200 or FITC-anti–mouse, dilution 1:50; purchased from Jackson ImmunoResearch Laboratories, Inc.) and TRITC-conjugated phalloidin (final of 2 µg/ml; Sigma-Aldrich) for 1 h at room temperature. Finally, the cells were washed with PBS and mounted on microscope slides using the ProLong Gold antifade reagent containing DAPI (Invitrogen). Images of the samples were taken using a widefield microscope (20× 0.7 NA air objective; DM6000B; Leica) equipped with a charge-coupled device camera (C10600 ORCA-R^{2}; Hamamatsu Photonics) using MM AF Premier software (Leica) or a A1R confocal microscope (10× 0.3 NA air or 60× 1.4 NA oil objective; NIS-Elements software), and were processed with ImageJ, Photoshop, and Illustrator.

Quantification of the data

ImageJ was used for all the measurements described below.

Blind analyses. Quantification of the formation of actin puncta, cable, and protrusions as well as AJ bulbs and also semiquantification of GFP-Dia accumulation at wound edge junction (Fig. 6 C) were performed blind. Before the quantification, each single image was randomly renamed using an ImageJ macro based on the "random" and "rename()" commands, so that the examiner was unaware of the sample or time point being quantified.

Quantification of actin puncta, cable, and protrusions. The following values in each image were measured: the total length of the wound edge (l_E [micrometers]), the number of the actin puncta at wound edge (n_p), the length of the wound edge covered by actin cable (l_C [micrometers]), or by the bases of lamellipodial and filopodial protrusions (l_P [micrometers]). Actin puncta were defined as F-actin spots at the wound edge that were (a) brighter or thicker than the cortical actin elsewhere in the cell and (b) had a long axis/short axis ratio of less than ∼2 (by visual inspection). Actin cables were defined as F-actin structures at the wound edge that were (a) brighter or thicker than the cortical actin elsewhere in the cell, (b) had a long axis/short axis ratio of greater than ∼2, and (c) had a smooth cytoplasmic edge. The entire wound edge, actin puncta, cable, and protrusion bases were manually marked using the freehand region of interest and pen tools of ImageJ. Then, the aforementioned values were measured. From these values, the following parameters to indicate the extent of puncta/cable/protrusion formation were obtained: puncta formation index = $100 \times n_p/l_E$ = the number of puncta per 100 µm of wound edge; cable formation index = $100 \times l_C/l_E$ = the percentage of wound edge occupied by cable; protrusion formation index = $100 \times l_P/l_E$ = the percentage of wound edge occupied by protrusions.

Accumulation of GFP-Dia at wound edge junctions. Semiquantification based on visual inspection: Wound edge junctions were scored as positive for GFP-Dia accumulation if their fluorescence level was greater in size or/and intensity than that of all vertices of the cell behind the wound edge. The percentage of wound edge junctions scoring positive in each image was calculated, and the means ± SEM of the percentages were plotted in Fig. 6 C.

Measurement of fluorescence intensity: The fluorescence of GFP-Dia at each wound edge junction was quantified. To correct the effect of photobleaching, the value was divided by the mean fluorescent intensity of entire image (512 pixels = 53.4-µm square). Finally, for each junction, these corrected values at each time point were normalized against the intensity before wounding. The means ± SEM of the resultant normalized intensity were plotted in Fig. 6 D.

Formation of AJ bulbs. Wound edge junctions were scored as positive for AJ bulb formation if their E-cadherin–GFP fluorescence is wider or brighter than that of the cell edges they connect. The percentage of wound edge junctions scoring positive in each image was calculated, and the means ± SEM of the percentages was plotted in Fig. 7 B.

Wound area (*Drosophila* embryos). We used the wounds whose size at 5 min after wounding was within the range of 200–1,000 μm^2, as they healed in a largely reproducible time course. For each wound, wound area was normalized to the value at 5 min after wounding (Fig. 1 F).

Wound width (scratch assay). Photographs of the wounds were taken so that the wound runs horizontally in the image. The area of wound within the image was then measured and divided by the image width to obtain mean wound width. The mean wound width for each single image was plotted in Fig. 8 D.

Graphs and statistical analyses

Prism (GraphPad Software) was used for statistical analyses and drawing graphs. Column scatter graphs and box–whisker plots were used to display the data at a single time point, and line plots were used for time courses. In the column scatter graphs, each data value from all the repeated experiments is plotted, and bars indicate the means ± SEM of all plotted values. In box–whisker plots, bars show minimum, maximum, and median, and boxes extend from the 25th to 75th percentiles. Line plots show the means ± SEM of all the individual data from repeated experiments unless otherwise stated. The total numbers of the samples (n) measured to obtain each single mean value are shown in the figure legends. The data shown in column scatter graphs and box–whisker plots were analyzed by the Mann–Whitney test. The time course data were analyzed by the Wilcoxon matched-pairs signed rank test, in which the mean values in each single experiment from at least three repeats were paired. If necessary, the Bonferroni correction for multiple comparisons was performed.

Online supplemental material

Fig. S1 shows that RNAi-mediated knockdown of *sra1*, a gene encoding a regulatory subunit of the SCAR complex, produces results consistent with those obtained for $SCAR^{\Delta 37}$ mutants (Fig. 2). Fig. S2 shows the result of the quantification of the fluorescence intensity of wound edge F-actin and cortical actin behind the edge in control and dia^5 M/Z embryos. Fig. S3 shows that accumulation of myosin II heavy chain at wound edges is reduced in shi^2 embryos; however, denticle development is not perturbed. Fig. S4 shows the localization of GFP-DiaΔ-DAD during wound closure. Table S1 summarizes the genotypes of the embryos used in each experiment. Video 1 shows the dynamics of actin and myosin at the wound edge. Video 2 shows the dynamics of actin during wound healing in control and $SCAR^{\Delta 37}$ embryos. Video 3 shows the dynamics of actin during wound healing in control and dia^5 M/Z embryos. Video 4 shows the dynamics of actin and Dynamin during wound healing. Video 5 shows the dynamics of actin during wound healing in control and shi^2 embryos. Video 6 shows the dynamics of actin during wound healing in control and Rab5DN-expressing embryos. Online supplemental material is available at http://www.jcb.org/cgi/content/full/jcb.201411037/DC1.

Acknowledgments

We thank Richa Rikhy, Jennifer Lippincott-Schwartz, Brian Stramer, and Martin Baron for providing fly stocks. We are grateful to Brian Stramer, Sarah Woolner, and Shirin Pocha for critically reading this manuscript and to the Faculty of Life Sciences and Bioimaging and Fly facilities for technical assistance.

This research was supported by Biotechnology and Biological Sciences Research Council grant BB/I007288/1 and Healing Foundation fellowship to T.H. Millard.

The authors declare no competing financial interests.

Submitted: 11 November 2014
Accepted: 24 June 2015

References

Abreu-Blanco, M.T., J.M. Verboon, R. Liu, J.J. Watts, and S.M. Parkhurst. 2012. *Drosophila* embryos close epithelial wounds using a combination of cellular protrusions and an actomyosin purse string. *J. Cell Sci.* 125:5984–5997. http://dx.doi.org/10.1242/jcs.109066

Afshar, K., B. Stuart, and S.A. Wasserman. 2000. Functional analysis of the *Drosophila* diaphanous FH protein in early embryonic development. *Development.* 127:1887–1897.

Antunes, M., T. Pereira, J.V. Cordeiro, L. Almeida, and A. Jacinto. 2013. Coordinated waves of actomyosin flow and apical cell constriction immediately after wounding. *J. Cell Biol.* 202:365–379. http://dx.doi.org/10.1083/jcb.201211039

Bement, W.M., P. Forscher, and M.S. Mooseker. 1993. A novel cytoskeletal structure involved in purse string wound closure and cell polarity maintenance. *J. Cell Biol.* 121:565–578. http://dx.doi.org/10.1083/jcb.121.3.565

Ben-Yaacov, S., R. Le Borgne, I. Abramson, F. Schweisguth, and E.D. Schejter. 2001. Wasp, the *Drosophila* Wiskott-Aldrich syndrome gene homologue, is required for cell fate decisions mediated by Notch signaling. *J. Cell Biol.* 152:1–13. http://dx.doi.org/10.1083/jcb.152.1.1

Brust-Mascher, I., and J.M. Scholey. 2009. Microinjection techniques for studying mitosis in the *Drosophila* melanogaster syncytial embryo. *J. Vis. Exp.* 31:1382.

Carvalho, L., A. Jacinto, and N. Matova. 2014. The Toll/NF-κB signaling pathway is required for epidermal wound repair in *Drosophila*. *Proc. Natl. Acad. Sci. USA.* 111:E5373–E5382. http://dx.doi.org/10.1073/pnas.1408224111

Chou, T.B., and N. Perrimon. 1996. The autosomal FLP-DFS technique for generating germline mosaics in *Drosophila melanogaster. Genetics.* 144:1673–1679.

Danjo, Y., and I.K. Gipson. 1998. Actin 'purse string' filaments are anchored by E-cadherin-mediated adherens junctions at the leading edge of the epithelial wound, providing coordinated cell movement. *J. Cell Sci.* 111:3323–3332.

Dutta, D., J.W. Bloor, M. Ruiz-Gomez, K. VijayRaghavan, and D.P. Kiehart. 2002. Real-time imaging of morphogenetic movements in *Drosophila* using Gal4-UAS-driven expression of GFP fused to the actin-binding domain of moesin. *Genesis.* 34:146–151. http://dx.doi.org/10.1002/gene.10113

Eden, S., R. Rohatgi, A.V. Podtelejnikov, M. Mann, and M.W. Kirschner. 2002. Mechanism of regulation of WAVE1-induced actin nucleation by Rac1 and Nck. *Nature.* 418:790–793. http://dx.doi.org/10.1038/nature00859

Entchev, E.V., and M.A. González-Gaitán. 2002. Morphogen gradient formation and vesicular trafficking. *Traffic.* 3:98–109. http://dx.doi.org/10.1034/j.1600-0854.2002.030203.x

Evans, I.R., J. Zanet, W. Wood, and B.M. Stramer. 2010. Live imaging of *Drosophila* melanogaster embryonic hemocyte migrations. *J. Vis. Exp.* 36:1696.

Fenteany, G., P.A. Janmey, and T.P. Stossel. 2000. Signaling pathways and cell mechanics involved in wound closure by epithelial cell sheets. *Curr. Biol.* 10:831–838. http://dx.doi.org/10.1016/S0960-9822(00)00579-0

Ferguson, S.M., and P. De Camilli. 2012. Dynamin, a membrane-remodelling GTPase. *Nat. Rev. Mol. Cell Biol.* 13:75–88.

Fernandez-Gonzalez, R., and J.A. Zallen. 2013. Wounded cells drive rapid epidermal repair in the early *Drosophila* embryo. *Mol. Biol. Cell.* 24:3227–3237. http://dx.doi.org/10.1091/mbc.E13-05-0228

Franke, J.D., R.A. Montague, and D.P. Kiehart. 2005. Nonmuscle myosin II generates forces that transmit tension and drive contraction in multiple tissues during dorsal closure. *Curr. Biol.* 15:2208–2221. http://dx.doi.org/10.1016/j.cub.2005.11.064

Geiger, J.A., L. Carvalho, I. Campos, A.C. Santos, and A. Jacinto. 2011. Hole-in-one mutant phenotypes link EGFR/ERK signaling to epithelial tissue repair in *Drosophila. PLoS ONE.* 6:e28349. http://dx.doi.org/10.1371/journal.pone.0028349

Georgiou, M., E. Marinari, J. Burden, and B. Baum. 2008. Cdc42, Par6, and aPKC regulate Arp2/3-mediated endocytosis to control local adherens junction stability. *Curr. Biol.* 18:1631–1638. http://dx.doi.org/10.1016/j.cub.2008.09.029

Harris, T.J. 2012. Adherens junction assembly and function in the *Drosophila* embryo. *Int Rev Cell Mol Biol.* 293:45–83. http://dx.doi.org/10.1016/B978-0-12-394304-0.00007-5

Homem, C.C.F., and M. Peifer. 2008. Diaphanous regulates myosin and adherens junctions to control cell contractility and protrusive behavior during morphogenesis. *Development.* 135:1005–1018. http://dx.doi.org/10.1242/dev.016337

Homem, C.C.F., and M. Peifer. 2009. Exploring the roles of diaphanous and enabled activity in shaping the balance between filopodia and lamellipodia. *Mol. Biol. Cell.* 20:5138–5155. http://dx.doi.org/10.1091/mbc.E09-02-0144

Ikenouchi, J., M. Furuse, K. Furuse, H. Sasaki, S. Tsukita, and S. Tsukita. 2005. Tricellulin constitutes a novel barrier at tricellular contacts of epithelial cells. *J. Cell Biol.* 171:939–945. http://dx.doi.org/10.1083/jcb.200510043

Ishihara, S., and K. Sugimura. 2012. Bayesian inference of force dynamics during morphogenesis. *J. Theor. Biol.* 313:201–211. http://dx.doi.org/10.1016/j.jtbi.2012.08.017

Jacinto, A., W. Wood, T. Balayo, M. Turmaine, A. Martinez-Arias, and P. Martin. 2000. Dynamic actin-based epithelial adhesion and cell matching during *Drosophila* dorsal closure. *Curr. Biol.* 10:1420–1426. http://dx.doi.org/10.1016/S0960-9822(00)00796-X

Kiehart, D.P., C.G. Galbraith, K.A. Edwards, W.L. Rickoll, and R.A. Montague. 2000. Multiple forces contribute to cell sheet morphogenesis for dorsal closure in *Drosophila. J. Cell Biol.* 149:471–490. http://dx.doi.org/10.1083/jcb.149.2.471

Kim, Y.T., and C.F. Wu. 1990. Allelic interactions at the shibire locus of *Drosophila*: effects on behavior. *J. Neurogenet.* 7:1–14. http://dx.doi.org/10.3109/01677069009084149

Krause, M., and A. Gautreau. 2014. Steering cell migration: lamellipodium dynamics and the regulation of directional persistence. *Nat. Rev. Mol. Cell Biol.* 15:577–590. http://dx.doi.org/10.1038/nrm3861

Kunda, P., G. Craig, V. Dominguez, and B. Baum. 2003. Abi, Sra1, and Kette control the stability and localization of SCAR/WAVE to regulate the formation of actin-based protrusions. *Curr. Biol.* 13:1867–1875. http://dx.doi.org/10.1016/j.cub.2003.10.005

Lee, T., and L. Luo. 1999. Mosaic analysis with a repressible cell marker for studies of gene function in neuronal morphogenesis. *Neuron.* 22:451–461. http://dx.doi.org/10.1016/S0896-6273(00)80701-1

Leibfried, A., R. Fricke, M.J. Morgan, S. Bogdan, and Y. Bellaiche. 2008. *Drosophila* Cip4 and WASp define a branch of the Cdc42-Par6-aPKC pathway regulating E-cadherin endocytosis. *Curr. Biol.* 18:1639–1648. http://dx.doi.org/10.1016/j.cub.2008.09.063

Levayer, R., A. Pelissier-Monier, and T. Lecuit. 2011. Spatial regulation of Dia and Myosin-II by RhoGEF2 controls initiation of E-cadherin endocytosis during epithelial morphogenesis. *Nat. Cell Biol.* 13:529–540. http://dx.doi.org/10.1038/ncb2224

Lye, C.M., H.W. Naylor, and B. Sanson. 2014. Subcellular localisations of the CPTI collection of YFP-tagged proteins in *Drosophila* embryos. *Development.* 141:4006–4017. http://dx.doi.org/10.1242/dev.111310

Macia, E., M. Ehrlich, R. Massol, E. Boucrot, C. Brunner, and T. Kirchhausen. 2006. Dynasore, a cell-permeable inhibitor of dynamin. *Dev. Cell.* 10:839–850. http://dx.doi.org/10.1016/j.devcel.2006.04.002

Marois, E., A. Mahmoud, and S. Eaton. 2006. The endocytic pathway and formation of the Wingless morphogen gradient. *Development.* 133:307–317. http://dx.doi.org/10.1242/dev.02197

Martin, P., and S.M. Parkhurst. 2004. Parallels between tissue repair and embryo morphogenesis. *Development.* 131:3021–3034. http://dx.doi.org/10.1242/dev.01253

Mateus, A.M., N. Gorfinkiel, S. Schamberg, and A. Martinez Arias. 2011. Endocytic and recycling endosomes modulate cell shape changes and tissue behaviour during morphogenesis in *Drosophila. PLoS ONE.* 6:e18729. http://dx.doi.org/10.1371/journal.pone.0018729

Matsubayashi, Y., and T.H. Millard. 2013. Developmental models for wound healing. *In* eLS. John Wiley & Sons, Ltd, Chichester, England, UK. http://dx.doi.org/10.1002/9780470015902.a0021306

Matsubayashi, Y., W. Razzell, and P. Martin. 2011. 'White wave' analysis of epithelial scratch wound healing reveals how cells mobilise back from the leading edge in a myosin-II-dependent fashion. *J. Cell Sci.* 124:1017–1021. http://dx.doi.org/10.1242/jcs.080853

Mattila, P.K., and P. Lappalainen. 2008. Filopodia: molecular architecture and cellular functions. *Nat. Rev. Mol. Cell Biol.* 9:446–454. http://dx.doi.org/10.1038/nrm2406

Miaczynska, M., L. Pelkmans, and M. Zerial. 2004. Not just a sink: endosomes in control of signal transduction. *Curr. Opin. Cell Biol.* 16:400–406. http://dx.doi.org/10.1016/j.ceb.2004.06.005

Millard, T.H., and P. Martin. 2008. Dynamic analysis of filopodial interactions during the zippering phase of *Drosophila* dorsal closure. *Development.* 135:621–626. http://dx.doi.org/10.1242/dev.014001

Millard, T.H., S.J. Sharp, and L.M. Machesky. 2004. Signalling to actin assembly via the WASP (Wiskott-Aldrich syndrome protein)-family proteins and the Arp2/3 complex. *Biochem. J.* 380:1–17. http://dx.doi.org/10.1042/BJ20040176

Myster, S.H., R. Cavallo, C.T. Anderson, D.T. Fox, and M. Peifer. 2003. *Drosophila* p120catenin plays a supporting role in cell adhesion but is not an essential adherens junction component. *J. Cell Biol.* 160:433–449. http://dx.doi.org/10.1083/jcb.200211083

Oda, H., and S. Tsukita. 2001. Real-time imaging of cell-cell adherens junctions reveals that *Drosophila* mesoderm invagination begins with two phases of apical constriction of cells. *J. Cell Sci.* 114:493–501.

Oda, Y., T. Otani, J. Ikenouchi, and M. Furuse. 2014. Tricellulin regulates junctional tension of epithelial cells at tricellular contacts through Cdc42. *J. Cell Sci.* 127:4201–4212. http://dx.doi.org/10.1242/jcs.150607

Olkkonen, V.M., and H. Stenmark. 1997. Role of Rab GTPases in membrane traffic. *Int. Rev. Cytol.* 176:1–85. http://dx.doi.org/10.1016/S0074-7696(08)61608-3

Pickering, K., J. Alves-Silva, D. Goberdhan, and T.H. Millard. 2013. Par3/Bazooka and phosphoinositides regulate actin protrusion formation during *Drosophila* dorsal closure and wound healing. *Development.* 140:800–809. http://dx.doi.org/10.1242/dev.089557

Rauchman, M.I., S.K. Nigam, E. Delpire, and S.R. Gullans. 1993. An osmotically tolerant inner medullary collecting duct cell line from an SV40 transgenic mouse. *Am. J. Physiol.* 265:F416–F424.

Razzell, W., W. Wood, and P. Martin. 2014. Recapitulation of morphogenetic cell shape changes enables wound re-epithelialisation. *Development.* 141:1814–1820. http://dx.doi.org/10.1242/dev.107045

Rikhy, R., M. Mavrakis, and J. Lippincott-Schwartz. 2015. Dynamin regulates metaphase furrow formation and plasma membrane compartmentalization in the syncytial *Drosophila* embryo. *Biol. Open.* 4:301–311. http://dx.doi.org/10.1242/bio.20149936

Sadowski, L., I. Pilecka, and M. Miaczynska. 2009. Signaling from endosomes: location makes a difference. *Exp. Cell Res.* 315:1601–1609. http://dx.doi.org/10.1016/j.yexcr.2008.09.021

Salazar, M.A., A.V. Kwiatkowski, L. Pellegrini, G. Cestra, M.H. Butler, K.L. Rossman, D.M. Serna, J. Sondek, F.B. Gertler, and P. De Camilli. 2003. Tuba, a novel protein containing bin/amphiphysin/Rvs and Dbl homology domains, links dynamin to regulation of the actin cytoskeleton. *J. Biol. Chem.* 278:49031–49043. http://dx.doi.org/10.1074/jbc.M308104200

Schäfer, G., S. Weber, A. Holz, S. Bogdan, S. Schumacher, A. Müller, R. Renkawitz-Pohl, and S.-F. Önel. 2007. The Wiskott-Aldrich syndrome protein (WASP) is essential for myoblast fusion in *Drosophila*. *Dev. Biol.* 304:664–674. http://dx.doi.org/10.1016/j.ydbio.2007.01.015

Schulte, J., U. Tepass, and V.J. Auld. 2003. Gliotactin, a novel marker of tricellular junctions, is necessary for septate junction development in *Drosophila*. *J. Cell Biol.* 161:991–1000. http://dx.doi.org/10.1083/jcb.200303192

Shaw, T., and P. Martin. 2009. Epigenetic reprogramming during wound healing: loss of polycomb-mediated silencing may enable upregulation of repair genes. *EMBO Rep.* 10:881–886. http://dx.doi.org/10.1038/embor.2009.102

Shimizu, H., S. Kawamura, and K. Ozaki. 2003. An essential role of Rab5 in uniformity of synaptic vesicle size. *J. Cell Sci.* 116:3583–3590. http://dx.doi.org/10.1242/jcs.00676

Tsarouhas, V., L. Yao, and C. Samakovlis. 2014. Src kinases and ERK activate distinct responses to Stitcher receptor tyrosine kinase signaling during wound healing in *Drosophila*. *J. Cell Sci.* 127:1829–1839. http://dx.doi.org/10.1242/jcs.143016

Wang, S., V. Tsarouhas, N. Xylourgidis, N. Sabri, K. Tiklová, N. Nautiyal, M. Gallio, and C. Samakovlis. 2009. The tyrosine kinase Stitcher activates Grainy head and epidermal wound healing in *Drosophila*. *Nat. Cell Biol.* 11:890–895. http://dx.doi.org/10.1038/ncb1898

Wood, W., A. Jacinto, R. Grose, S. Woolner, J. Gale, C. Wilson, and P. Martin. 2002. Wound healing recapitulates morphogenesis in *Drosophila* embryos. *Nat. Cell Biol.* 4:907–912. http://dx.doi.org/10.1038/ncb875

Wu, Y., M. Eghbali, J. Ou, R. Lu, L. Toro, and E. Stefani. 2010. Quantitative determination of spatial protein-protein correlations in fluorescence confocal microscopy. *Biophys. J.* 98:493–504. http://dx.doi.org/10.1016/j.bpj.2009.10.037

Zallen, J.A., Y. Cohen, A.M. Hudson, L. Cooley, E. Wieschaus, and E.D. Schejter. 2002. SCAR is a primary regulator of Arp2/3-dependent morphological events in *Drosophila*. *J. Cell Biol.* 156:689–701. http://dx.doi.org/10.1083/jcb.200109057

Zulueta-Coarasa, T., M. Tamada, E.J. Lee, and R. Fernandez-Gonzalez. 2014. Automated multidimensional image analysis reveals a role for Abl in embryonic wound repair. *Development.* 141:2901–2911. http://dx.doi.org/10.1242/dev.106898